ISSN 1063-7842, Technical Physics, 2015, Vol. 60, No. 5, pp. 686–694. © Pleiades Publishing, Ltd., 2015.
Original Russian Text © S.V. Ovchinnikov, A.D. Korotaev, Yu.P. Pinzhin, 2015, published in Zhurnal Tekhnicheskoi Fiziki, 2015, Vol. 85, No. 5, pp. 57–65.

PHYSICAL SCIENCE OF MATERIALS

Structure of Ti–Al–Si–N Gradient Coatings

S. V. Ovchinnikov[a], A. D. Korotaev[b], and Yu. P. Pinzhin[a]

[a] *Institute of Strength Physics and Materials Science, Siberian Branch, Russian Academy of Sciences, pr. Akademicheskii 2/4, Tomsk, 634021 Russia*

[b] *Tomsk State University, pr. Lenina 36, Tomsk, 634050 Russia*

e-mail: ovm@spti.tsu.ru

Received July 30, 2014

Abstract—The microstructure, the stresses, and the elemental composition of Ti–Al–Si–N gradient coatings are studied by transmission electron microscopy and electron-probe microanalysis of thin foils prepared in the cross section of the coatings. As the concentration of the elements that alloy titanium nitride increases across the coating thickness, the structure of the coating changes from submicrocrystalline columnar grains to nanocrystalline grains. In these structural states, the structural characteristics (lattice parameter, lattice bending–torsion, crystal size, type of intragranular defect structure) and the residual stresses change. The magnitude and the sign of residual stresses change when the type of structural state changes.

DOI: 10.1134/S1063784215050205

INTRODUCTION

The formation of composition-gradient coatings is one of the promising trends in synthesizing functional, e.g., wear-resistant and protective, coatings for cutting tool [1]. The results of practical application of such coatings demonstrate the possibility of up to a tenfold increase in the wear resistance of the cutting tool [2, 3]. Gradient coatings also exhibit high characteristics in traditional scratch and tribological tests [4–6].

As noted in those works, the factors that determine an increase in the characteristics of gradient coatings are an increase in their adhesion due to a decrease in the difference between the physical and mechanical properties of a substrate and a coating, the redistribution of residual stresses in a coating, an increase in the strength of the coating due to the creation of a heterophase or layered structure, and a decrease in the friction forces on the coating surface because of the presence of a high volume fraction of an antifriction phase (carbon, Mo and W dichalcogenides) in the surface layer. Of course, the action of these factors is obvious under proper conditions, which is supported by both theoretical calculations and experimental measurements [7, 8].

It is also obvious that these factors are related to microstructure features, and the formation of a certain structural state and the possibilities of its change in the element system used for a coating is necessary for their effective operation under operating conditions. It should be noted that the structural state of gradient coatings were studied with direct analysis methods, such as transmission electron microscopy, in a few works [4, 9–12].

The authors of those works mainly investigated phase transformations (only the shape and size of coherent domains was only noted among the structural characteristics) in relatively "simple" systems consisting of a few elements due to creating the gradient of nitrogen [4, 9], nitrogen with carbon [3, 11], or one of the phase-forming elements (Cr, Al [8, 12]) having a sufficiently significant solubility in titanium nitride–based coatings. This approach cannot be used to form multiphase system and to determine the change of the structural parameters as a function of the alloying element (AE) concentration. Therefore (due to a wide use of one-layer coatings of similar compositions), it is interesting to study coatings with gradients of the elements that can effectively change the structure, the phase composition, and the strength and tribological properties of the coatings. The purpose of this work is to study the Ti–Al–Si–N system, since it meets these conditions. Changes in the structure of gradient Ti–Al–Si–N coatings (thickness gradient of the Al and Si concentrations) were investigated using dark-field electron-microscopic analysis of the cross sections of thin foils.

EXPERIMENTAL

Ti–Al–Si–N coatings were formed by reactive magnetron sputtering of Ti (VT1-0 alloy) and Al–Si alloy (silumin containing 12 at % Si) targets in an argon or nitrogen medium under conditions of two assisted sources of gas (nitrogen) plasma onto substrates made of molybdenum or a T15K6 hard alloy during their planetary rotation at a rate of 12 rpm and an argon to nitrogen flux ratio of 3 : 1. Before deposition, the substrates were electrolytically (mechanically) polished and then subjected to ultrasonic cleaning in ethyl alcohol. We then performed the following

operations: cleaning and heating of the substrate surface by argon ions at a bias voltage $U_s = -350$ V and the deposition of a titanium sublayer with its nitriding in a nitrogen gas discharge at a negative bias voltage of 6 kV applied to the substrate.

The coatings were grown at a pulsed (pulse frequency and duration of 10 kHz and 50 μs, respectively) bias voltage $U_s = -200$ V and a deposition temperature of ~180°C. The magnetron power supply powers were 1.8 kW for a titanium target and 0.2–1.40 kW for an Al–Si alloy, and the gas nitrogen source power was 0.7 kW. TiN was first deposited onto a nitrided titanium sublayer for 30 min, and layers of an alloyed coating with changing element concentrations were then deposited onto TiN due to an increase in the power of sputtering a silumin target by 0.1 kW per 5 min. The synthesis of a layer with the maximum silumin sputtering power was performed during 1 h. The rate of nitrogen leak increased in proportion to an increase in the target sputtering power. The total deposition time and the thickness of the layer with the sublayer were 150 min and 1.9 μm, respectively.

Electron-probe microanalysis (EPMA) of the elemental compositions of the coatings and structural investigations were carried out by electron-microscopic analysis on the Philips SEM-515 and Philips CM-12 electron microscopes of the Materials Science Center for Joint Use of Tomsk State University and the JEM-2100 electron microscope of the Center for Joint Use Nanotekh of Institute of Strength Physics and Materials Science, Siberian Branch, Russian Academy of Sciences.

EXPERIMENTAL RESULTS

Based on the times of deposition of layers at various Al–Si target sputtering powers (or the measured depth profiles of the AE concentrations), we can estimate the layer thicknesses in a coating. This estimate demonstrates that the TiN layer is located at a distance of 400 nm from the substrate surface, the alloyed layer with a changing element concentration is located at a distance of 1050 nm, and the layer with a constant element concentration is located at a distance of 1050 nm from the coating surface.

The results of measuring the elemental composition of a bulk sample, i.e., the results averaged over the coating thickness, give the following concentrations (at %): 24.6 Ti, 25.3 Al, 2.2 Si, and 47.9 N. It is seen that the ratio of elements is close to the stoichiometric composition of compound (Ti, Al, Si)N the formation of which is supported by the electron diffraction patterns of a single-phase *B*1 solid solution in both the surface layer and throughout the coating thickness (Fig. 1a). It is obvious that the deviations from the stoichiometry of this compound cannot go outside its homogeneity area and are likely to be smaller than the presented data because of decreasing the contents of the elements that correspond to the metallic sublattice in the solid solution due to, first, the segregation of the elements (silicon, aluminum) that are insoluble under equilibrium conditions and are weakly soluble under deposition conditions along the boundaries of growing crystals [13, 14] and, second, the presence of an insignificant formation of α-Ti that did not react with nitrogen [15]. Because of the well-known problems related to the EPMA determination of the concentrations of light elements, the element concentrations in the metallic sublattice are determined from the ratios of the corresponding element concentrations obtained by semiquantitative EPMA by normalizing them to the stoichiometry of the TiN compound.

It was found that the AE concentrations measured by EPMA in the cross section of thin foils in the regions corresponding to an increase in the silumin target sputtering power increases monotonically for Al and Si at least to the distances corresponding to the upper boundary of the region of transition from a submicrocrystalline into a nanocrystalline state (~950 nm; Figs. 1b, 1c). The differences in the distributions of these elements detected at large distances from the substrate are related to the behavior of the silicon concentration, namely, its drop and sharp growth in the nanocrystalline region next to the transition zone. At present, we have no experimental data to unambiguously explain these differences. They are likely to be associated with a change in the silicon sputtering rate after the end of silicon segregation along the boundaries of growing crystals and with the formation of a SiN_x layer. Here, we should note a relatively higher silicon content (with respect to aluminum) in the nanocrystalline region as compared to the submicrocrystalline region. In the surface nanocrystalline layer, we detected an oscillating character of the concentrations of both elements.

As noted above, the alloying elements used in this work have a limited solubility in the titanium nitride–based coatings synthesized by physical vapor deposition (PVD). The precipitation of one of them (Si) along the boundaries of growing crystals leads to a change in the growth mechanism and to the refinement of the coating structure to a nanograined state [13, 14]. This behavior is qualitatively supported by in our case when the growth macrostructure of the coatings was studied on their cross sections (Fig. 2a). The smooth surface of the cross section at the top of the coating (arrow *1*) indicates a more dispersed structure as compared to the layer that is closer to the substrate the relief of which is characteristic of a columnar structure (arrow *2*).

A more convincing indication of structural changes was obtained upon an electron-microscopic (transmission) investigation of the microstructure of the cross sections of the coatings. In particular, we detected characteristic growth structures: columnar submicrocrystalline grains (0.2–0.3 μm in size), nanocrystalline equiaxed grains, and a transition zone between them (Fig. 2b). Thus, the synthesized coat-

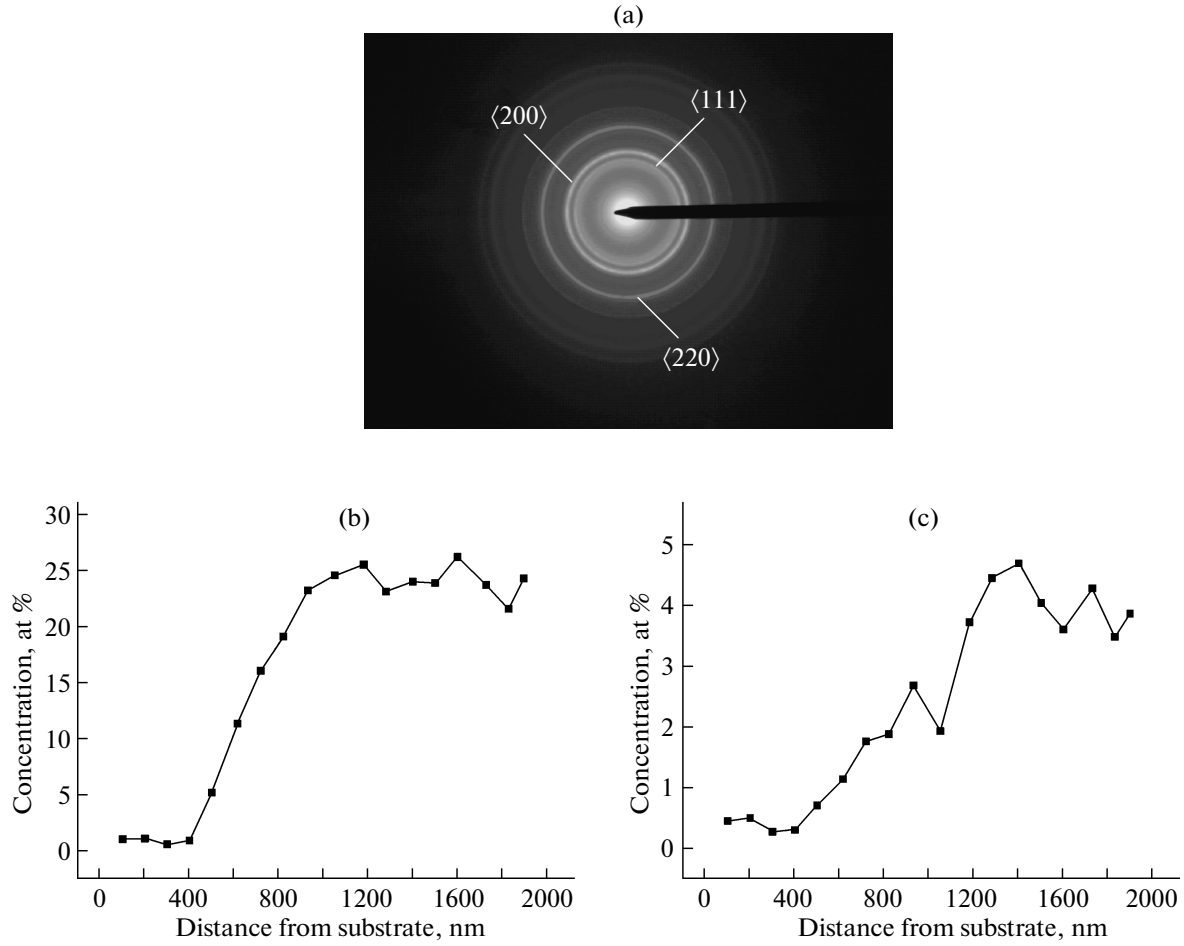

Fig. 1. (a) Electron diffraction pattern of the surface layer and the depth profiles of the concentration of (b) Al and (c) Si.

ings have a structure combining submicro- and nanocrystalline states, which can be useful for controlling the mechanical properties of the coatings by changing the ratio of the volume fractions of the structural constituents. In particular, the coating under study has a microhardness of about 33 GPa, which is higher than the hardness of plain titanium nitride (about 25 GPa [3, 10]) but is lower than that of the superhard coatings of this system [13].

Figure 2c shows that the change of the lattice parameter of titanium nitride in the coating zone with columnar grains has a nonmonotonic character with the maximum lattice parameters corresponding to the boundary of conjugation of the coating and the nitrided sublayer to the distance that approximately corresponds to the undoped titanium nitride thickness (~400 nm). The lattice parameter decreases with increasing AE concentration. The lattice parameter is close to the tabulated lattice parameter of undoped titanium nitride in the distance range 650–750 nm and decreases additionally by ≈0.007 nm at a longer distance from the substrate surface, in the nanocrystalline region next to the transition zone.

When studying the structure of the submicrocrystalline region in the gradient coating, we revealed the following features. First, a competitive character of the growth of columnar grains is observed up to the transition zone. This character manifests itself in a change of the columnar crystal size across the coating thickness (see arrows *1* (crystal is not in the reflecting position, and its diameter decreases with increasing thickness) and *2* (crystal is in the reflecting position, and its diameter increases with the thickness) in Fig. 3a) and in the presence of texture components in the electron diffraction patterns of the columnar structure (Fig. 3b). The calculation of the electron diffraction patterns demonstrates the existence of two zone axes, namely, {100} (bright ⟨200⟩ reflections) and {110} (⟨111⟩ reflections), and the dark-field image in Fig. 3a was taken with a reflection of the {100} texture component.

Second, the intragranular structure has a network of dislocations propagating at high (~80°) angles to crystal boundaries at distances between the dislocations of 10–15 nm, which corresponds to a scalar dislocation density of $(4–10) \times 10^{11}$ cm^{-2}. Dark-field

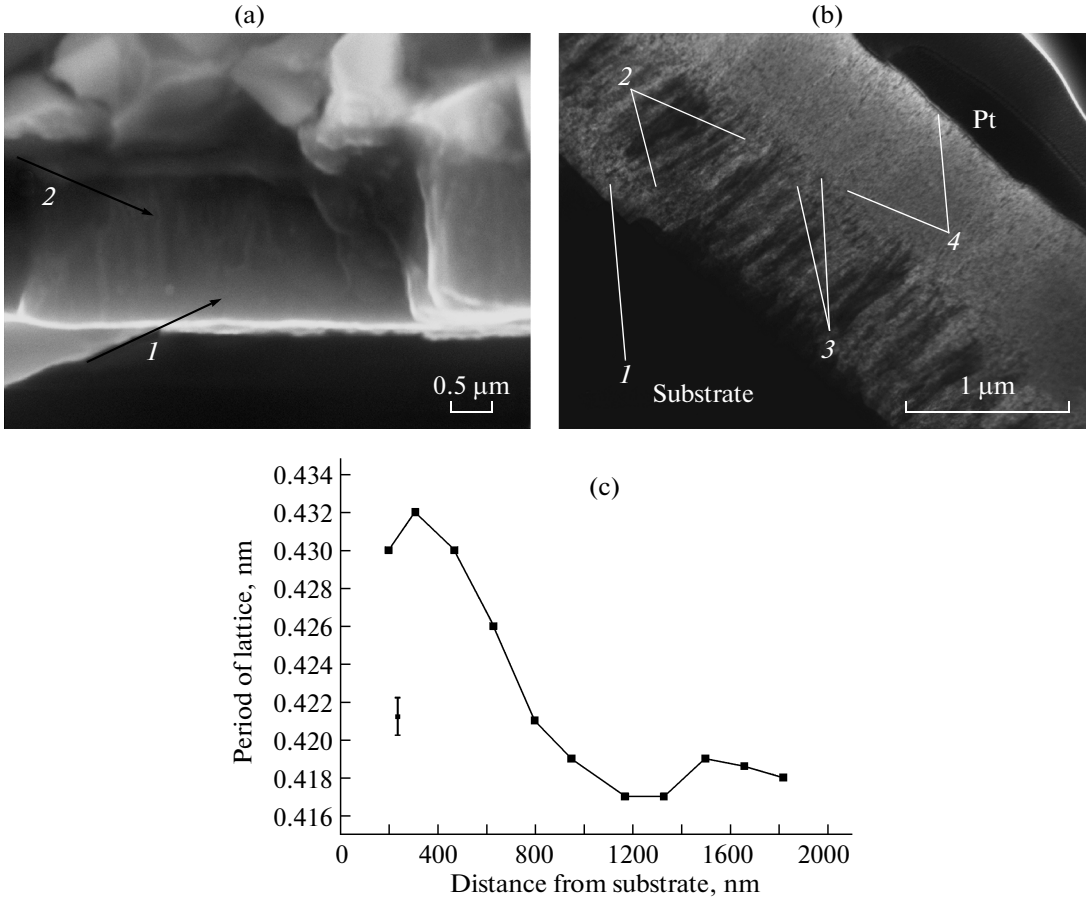

Fig. 2. Electron-microscopic images of the cross section of the coating in reflection geometry. (a) Fracture surface. (b) Arrow *1* indicates a nitrided sublayer; arrow *2*, submicrocrystalline structure boundaries; *3*, transition zone boundaries; and *4*, nanocrystalline region boundaries. (c) Lattice parameter of alloyed titanium nitride vs. the distance from the substrate surface.

electron-microscopic analysis of the bending–torsion of the crystal lattice shows that the dislocation structure has an excess density of dissociations of the same sign ($\rho_{\pm}$). This density is [16, 17]

$$\rho_{\pm} = \chi_{21}/b, \quad (1)$$

where χ_{21} is the bending–torsion tensor component related to the bending of the planes that are normal to the electron beam and b is the Burgers vector.

For example, Figs. 3c and 3d show dark-field images of the structure, which illustrate the motion of an extinction contour when the foil is tilted. The contour shifts from right to left and from top to bottom to the point indicated by arrow *1* when the foil is tilted by $\Delta\varphi \approx 0.5°$. This shift is $r = 7$ nm, which corresponds to $\chi_{21} = \Delta\varphi/r = 0.5°/7\ \text{nm} \approx 70°/\mu\text{m}$ and $\rho_{\pm} \approx 4 \times 10^{11}\ \text{cm}^{-2}$. Similar measurements and estimates demonstrate that the local quasi-continuous bending–torsion deformations of the crystal lattice weakly change across the coating thickness in the submicrocrystalline region: they are (60°–70°)/μm.

The character of the dislocation structure in crystals changes in the regions that are adjacent to the zone of transition into a nanocrystalline state. Specifically, long dislocation segments disappear and the dislocation tangle density increases (Fig. 3e, arrows). More pronounced low-angle fragmentation (fragments with a misorientation of 0.5° are shown by arrows *1* in Fig. 3f) with fragments several tens of nanometers in size is clearly visible as compared to the regions that are closer to the substrate. Some such fragments are elongated in the coating growth direction. Moreover, single low-angle boundaries with high misorientation angles, which are tilted and normal to the growth direction, appear (Fig. 3f, arrows *2*). Such boundaries are absent at a distance of 400–500 nm from the substrate surface.

The transition zone between the submicrocrystalline and nanocrystalline regions, which is detected at a distance of ~750–950 nm from the substrate surface and a silicon concentration of 1.9–2.65 at %, is visible due to an increase in the density of low-angle boundaries in it. These boundaries are elongated in the coating growth direction; that is, a nanocolumnar structure with a column diameter of 10–20 nm forms (Fig. 4a, some columnar crystals are indicated by arrows).

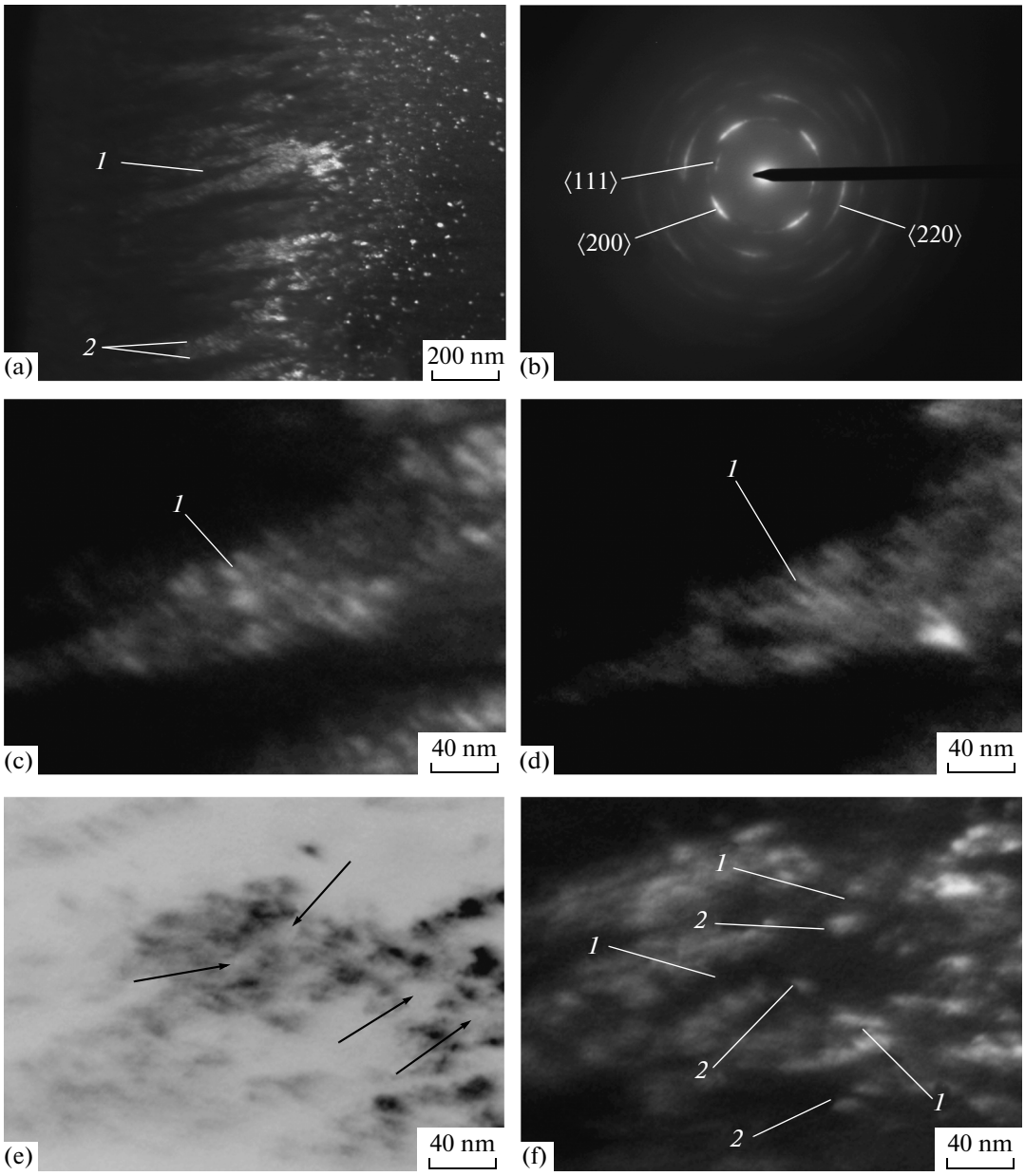

Fig. 3. (b) Electron diffraction pattern and dark-field images of the coating structure in the submicrocrystalline region ((e) negative image; see text).

In this structure, the boundaries along the growth direction and the boundaries that are perpendicular to them and are detected at the top of this region are low-angle boundaries, and one of the horizontal misorientation components is at most 3°. These misorientations divide elongated subgrains into low-angle fragments 20–60 nm in length.

The density of low-angle boundaries increases in the structure by a factor of 2–3 when the distance from the substrate surface increases by 150–200 nm. In the remaining part of the nanocrystalline region, the change in the average crystal sizes is insignificant (5 nm) with a minimum size of ≈8.5 nm at a distance of about 1500 nm from the substrate surface. In contrast to the transition zone and its adjacent regions, one of the horizontal misorientation vector components reaches 5°–6° in most fragment boundaries. A dark-field image shows a typical nanocrystalline structure (Fig. 4b, arrows *1* and *2* indicate individual crystals), and large crystals 40–50 nm in size are observed only in some regions (Fig. 4b; arrows *3*, *4)*. It is interesting that the lattice parameter of alloyed titanium nitride in the nanocrystalline region also changes nonmonotonically in the range 0.417–0.419 nm and reaches the maximum value at approximately the same distance where the crystal size is minimal (Fig. 2b).

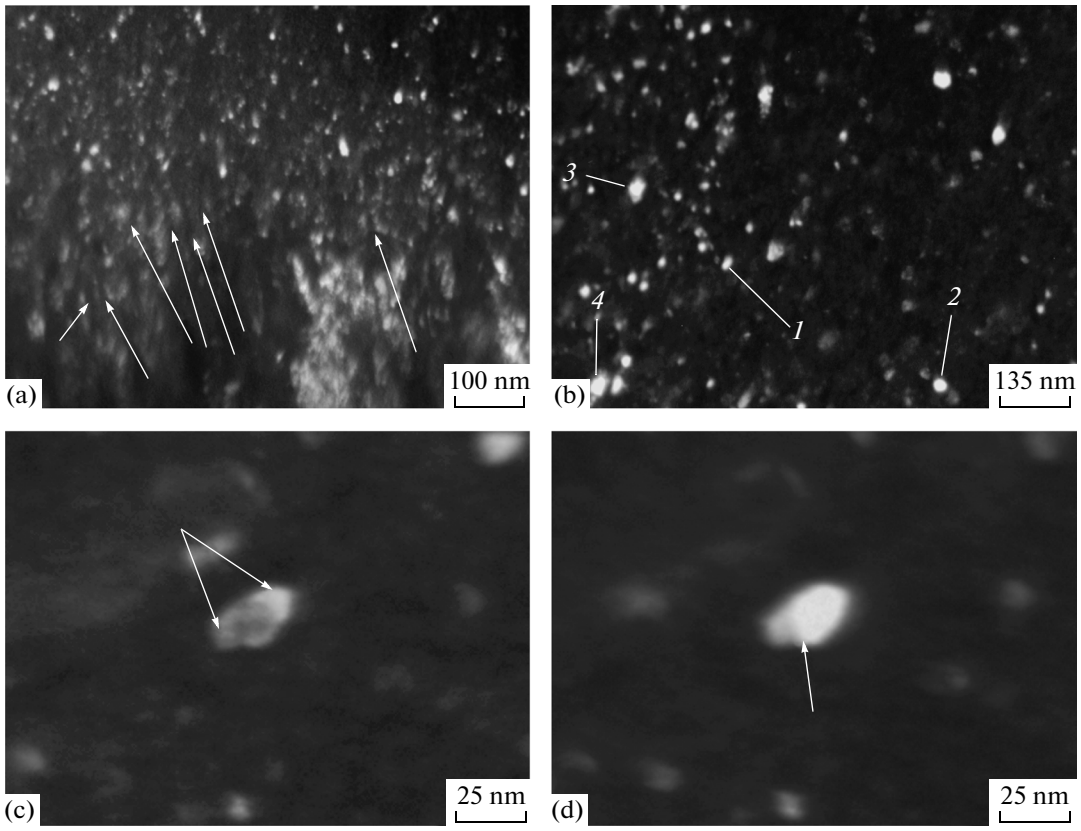

Fig. 4. Dark-field images of (a) transition zone, (b) nanocrystalline region, and (c, d) single nanocrystal at a goniometer tilt angle of (c) 0° and (d) 1°.

Using the dark-field electron-microscopic technique, we measured the bending–torsion of the crystal lattice in single nanocrystals in the nanocrystalline region (Figs. 4c, 4d). As follows from a comparison of the dark-field images, an extinction contour shifts from right to left and from top to bottom at a distance of about 10 nm at a tilt of 1°, which corresponds to the bending of $\chi_{21} = 1°/10\ \text{nm} \approx 100°/\mu\text{m}$ of the crystalline planes that are perpendicular to the electron beam. A comparison of the results of similar measurements performed in regions at various distances from the substrate surface demonstrates that, first, the average value of bending–torsion of the crystal lattice increases by 30–40% in transition from the submicrocrystalline to the nanocrystalline region and, second, these changes are qualitatively similar to the changes of the crystal sizes in the nanocrystalline region. In other words, the bending–torsion of the lattice and the crystal sizes decrease as the coating surface is approached. These changes have an oscillating character and correlate qualitatively with the silicon concentration in the surface layers of the nanocrystalline layer (Fig. 1c).

The study of the bending–torsion of the lattice in single crystals shows its complex character, which is nonuniform over the cross section. Quasi-continuous and discrete misorientations of fragments of 1° can be distinguished in some relatively large (25–30 nm) crystals, and one of the misorientations is indicated by the arrow in Fig. 4d. A characteristic example of such lattice misorientations inside a crystal is represented by the difference between the orientations of its center and periphery (see the arrows in Fig. 4c, which indicate the peripheral area in the reflecting position). The results of measuring the bending of the reflecting crystallographic planes that are parallel to the coating growth plane demonstrate that this bending in the peripheral area of crystals is higher by a factor of 2–3. The typical bending is (40°–50°)/μm for the center and up to 150°/μm in the peripheral area.

DISCUSSION OF RESULTS

Our results demonstrate a nonlinear character of changing the structural parameters (including their relation to deposition conditions) across the thickness of the gradient coating and their mutual influence. As for the change of the AE concentrations across the coating thickness, we note the following. It is seen in Figs. 1b and 1c that nonzero silicon and aluminum concentrations are detected at the nitrided sublayer α-Ti–TiN interface and in the titanium nitride layer, i.e., at a distance of several hundred nanometers from the beginning of the region alloyed with Al and Si.

According to the data on the diffusion mobility of AEs in titanium nitride at the deposition temperature [13, 18], the diffusion lengths of aluminum and silicon are much smaller than this distance. Therefore, the Al and Si contents (up to 0.6 and 0.3 at %, respectively) determined at a distance of 400–450 nm from the substrate surface are artifacts, which are likely to be related to the resputtering of part of coating material when the foil was prepared using a focused ion beam.

This consideration of the mutual influence structure–elemental composition demonstrates that it has no threshold character for the formation of nanograins. This effect takes place during the formation of a nanocolumnar structure, which is thought to be caused by the activation of surface silicon diffusion by an ion–plasma flux, since the bulk diffusion of silicon should favor three-dimensional nanostructure formation. However, the effect of the element concentrations on the structural characteristics on a microlevel (residual stresses, lattice parameter, coherent domain size) is monotonic and insignificant (in some ranges of the concentration region).

In particular, sharp structural changes across the coating thickness are not detected despite a steplike change in the silumin target sputtering power. This finding is likely to indicate relatively small strain and stress gradients in the alloyed layer with a submicrocrystalline structure that are induced by a substitutional impurity concentration gradient as compared to the residual stresses induced by larger structural defects. Here, we should note an extremely high scalar density and an excessive number of dislocations of the same sign inside columnar crystals. They determine relative constancy of the bending–torsion of the crystal lattice and local residual stresses across the zone with a submicrocrystalline structure.

The local residual stresses for elastoplastic lattice bending can be estimated from the relation [16, 17]

$$\sigma \approx E\chi_{ij}h/2, \quad (2)$$

where E is Young's modulus and h is the size of the dislocation charge that generates bending. When substituting $h \approx 0.1$ μm (foil thickness) into this relation, we find that the stress is $\sigma \approx E/15$. However, from lattice microstrain ε_p, we should expect much lower values,

$$\sigma \approx E\varepsilon_p = E\Delta a/a, \quad (3)$$

where a is the measured lattice parameter of alloyed nitride and $\Delta a = a - a_t$ is the change of the lattice parameter as compared to tabulated parameter a_t for titanium nitride.

Using the data in Fig. 2c and $a_t \approx 0.424$ nm, we obtain $\Delta a \approx 0.006$ nm and $\sigma \approx E/70$ for the region of undoped titanium nitride. Allowing for alloying with 15 at % Al at the boundary of the transition zone (effect of silicon is not taken into account because of its low content), which decreases the lattice parameter [19, 20], we should additionally decrease Δa by about 0.002 nm. This demonstrates that the averaged stresses at this distance are close to zero and that they decrease across the alloyed-layer thickness. The difference between the local stresses (from lattice bending) and the stresses averaged over scale up to 200 nm (region of microdiffraction) points to a nonuniform state of stress and absent long-range stress fields.

From the standpoint of structural characteristics, these features can be expressed in changing the localization size of the dislocation charge that induces bending. The dislocation contour in the dislocation structure under study is fragmented into chaotic regions up to 30 nm in size, and there is no regular (in one direction) motion, which is up to 10 nm, of the contour fragments when the foil is tilted. These findings are thought to indicate an orientation chaos and the localization of bending–torsion on the noted scales. Therefore, it seems reasonable to use $h \approx 10$–30 nm in Eq. (2), which gives the local stresses of the order of those determined from the lattice microstrain.

Thus, the relative constancy of the local stresses (from the lattice bending) and the decrease in the averaged stresses (from the lattice parameter) in the submicrocrystalline region correlate with the alloying-induced decrease in the lattice parameter in this region. Moreover, the detected changes in the dislocation structure and the appearance of scale fragmentation with increasing the AE concentrations in the submicrocrystalline region, which is next to the transition zone, are effects of increasing the heterogeneity, the scale, and the relaxation of local stresses.

The large lattice parameters (as compared to the tabulated data) at a distance up to 700 nm from the substrate surface, which are caused by the fact that the interplanar spacings of reflecting planes are measured in the cross section, point to the presence of residual stresses in the coating growth plane (Fig. 2c). As follows from Figs. 1 and 2 and the effect of AEs on the lattice parameter of alloyed titanium nitride [19, 20], its significant decrease (~0.007 nm) in the nanocrystalline region cannot be caused only by alloying. This means that the averaged stresses in the surface layer of this region are tensile and that they have the same order of magnitude as the compressive stresses in the submicrocrystalline region.

The presence of a transition from compressive to tensile stresses across the coating thickness suggests the existence of a zone where the stresses are close to zero. The distance from this zone to the substrate surface should correspond to the change of the lattice parameter from the value characteristic of undoped titanium nitride to the value only determined by alloying. As follows from [19, 20], the alloying-induced decrease in the lattice parameter is about 1% of the lattice parameter of undoped titanium nitride and changes weakly in the aluminum concentration range above 15 at % (for the silicon concentrations reached in this work, the decrease in the lattice parameter is at most 0.001 nm). Therefore, the distance at which the lattice parameter becomes smaller than 0.420 nm, is

taken to be the field of action of tensile stresses. As is seen in Fig. 2c, this distance is 850–900 nm; that is, it is in the zone of transition from a submicrocrystalline to a nanocrystalline state. Thus, a stress gradient should be at a distance of 700–850 nm from the substrate surface. According to [21], this gradient can additionally contribute to the diffusion of AEs: for example, it can favor the diffusion of silicon, as an impurity with a smaller atomic size as compared to titanium, from a tension to a compression zone, resulting in its nonuniform distribution in the zone adjacent to the transition zone (Fig. 1c).

Apart from the measured nonuniformities of a silicon distribution across the coating thickness, such nonuniformities are likely to take place in the cross section of single nanocrystals in the nanocrystalline region. This assumption can be based on the detected significant difference between the values of bending–torsion at the center and the periphery of crystals and on the specific features of this bending. It has a dipole character, which means that the orientation of reflecting planes changes symmetrically with respect to the center of a crystal (see [22, Fig. 8]). This dipole character of misorientation can be related to the defects of crystal boundaries, in particular, disclinations of opposite signs in opposite boundaries [17, 22]. The existence of such defects should lead to a gradient of their stresses across a crystal and to the corresponding impurity diffusion in the gradient field. For this structural model, we use the relation between disclination strength ω and stress σ

$$\sigma = G\omega/2\pi, \quad (4)$$

where G is the shear modulus, and estimate the stresses in the near-boundary regions for $\omega \approx \chi_{ij} d/2$, where $\chi_{ij} \approx 150^\circ/\mu m$ is the bending–torsion of the lattice in these regions and $d \approx 20$ nm is the crystal size. This calculation gives the stress of $G/240$. Moreover, the presence of heterogeneities, i.e., the gradients of distributions of impurities and point defects over the crystal volume, which are caused by the differences between their atomic volumes and the matrix atomic volume, can also similarly change the orientation of reflecting planes.

CONCLUSIONS

Based on the studies of the elemental and phase compositions and the structure of Ti–Al–Si–N gradient coatings, we can draw the following conclusions.

(1) It was shown that a change in the concentrations of weakly soluble (insoluble) impurities up to 10–15 at % Al and 2.6 at % Si weakly affected the structural parameters, namely, the coherent domain size and the bending–torsion of the crystal lattice, when the lattice parameter monotonically decreased in a submicrocrystalline state. An increase in the AE concentration leads to a change in the character of a dislocation structure and to the appearance of scale low-angle lattice fragmentation.

(2) When the lattice parameter and the AE concentration change, a gradient of residual stresses forms across a coating, and their sign changes from compressive to tensile stresses when the coating thickness increases.

(3) The AE (Al, Si) concentration at which the structure of a coating changes from a submicrocrystalline to a nanocrystalline state was determined. The structural transition from a submicrocrystalline to a nanocrystalline region was traced during the growth of gradient coatings, and this transition manifests itself in the formation of a nanocolumnar structure in the transition zone.

(4) The structure of nanocrystals is characterized by dipole misorientations in their cross section, which can be caused by the presence of defects of different signs at boundaries or by a nonuniform distribution of AEs and point defects in the crystal volume.

ACKNOWLEDGMENTS

This work was supported by the program of basic scientific research of state academies of sciences in 2013–2020, the program of enhancing the competitive ability of Tomsk State University, and the Russian Foundation for Basic Research (project no. 13-08-00502).

REFERENCES

1. C. Donnet and A. Erdemir, Surf. Coat. Technol. **180–181**, 76 (2004).
2. D. Loktev, Struzhka **2** (5), 12 (2004).
3. V. P. Tabakov, *Formation of Wear-Resistant Ion-Plasma Coatings for Cutting Tools* (Mashinostroenie, Moscow, 2008).
4. M. Zhang, M. K. Li, K. H. Kim, and F. Pan, Appl. Surf. Sci. **225**, 9200 (2009).
5. M. Antonov, I. Hussainova, F. Sergejev, P. Kulu, and A. Gregor, Wear **267**, 898 (2009).
6. S. PalDey and S. C. Deevi, Mat. Sci. Eng. A. Struct. **361**, 1 (2003).
7. X. C. Zhang, B. S. Xu, H. D. Wang, Y. X. Wu, and Y. Jiang, Mater. Des. **28**, 1192 (2007).
8. V. V. Uglov, V. M. Anishchik, S. V. Zlotski, G. Abadias, and S. N. Dub, Surf. Coat. Technol. **200**, 178 (2005).
9. H. Era, Y. Ide, A. Nino, and K. Kishitake, Surf. Coat. Technol. **194**, 265 (2005).
10. P. H. Mayrhofer, C. Mitterer, L. Hultman, and H. Clemens, Prog. Mater. Sci. **51**, 1032 (2006).
11. C. Fernandez-Ramos, J. C. Sanches-Lopez, A. Justo, T. C. Rojas, I. Papst, F. Hofer,and A. Fernandez, Surf. Coat. Technol. **180–181**, 526 (2004).
12. R. Manaila, A. Devenyi, D. Biro, L. David, P. B. Barna, and A. Kovacs, Surf. Coat. Technol. **151–152**, 21 (2002).

13. S. Veprek, M. G. J. Veprek-Heijman, P. Karvankova, and J. Prochazka, Thin Solid Films **476**, 1 (2005).
14. C. S. Sandu, R. Sanjines, M. Benkahoul, F. Medjani, and F. Levy, Surf. Coat. Technol. **201**, 4083 (2006).
15. S. V. Ovchinnikov, A. D. Korotaev, and Yu. P. Pinzhin, Deform. Razrush. Mater., No. 3, 24 (2014).
16. A. D. Korotaev, A. N. Tyumentsev, and V. F. Sukhovarov, *Dispersion Hardening of Refractory Metals* (Nauka, Novosibirsk, 1989).
17. A. N. Tyumentsev, A. D. Korotaev, and Yu. P. Pinzhin, Fiz. Mezomekh. **7** (4), 35 (2004).
18. L. Hultman, Vacuum **57**, 1 (2000).
19. F. Vaz, L. Rebouta, Ph. Goudeau, T. Girardeau, J. Pacaud, J. P. Riveire, and A. Traverse, Surf. Coat. Technol. **146–147**, 274 (2001).
20. *Nanostructured Coatings*, Ed. by A. Cavaleiro and J. Th. M. de Hosson (Springer, New York, 2006), pp. 261–314.
21. R. W. Cahn and P. Haasen, *Physical Metallurgy,* 3rd ed. (North Holland, Amsterdam, 1983), Vol. 2.
22. S. V. Ovchinnikov, A. D. Korotaev, V. Yu. Moshkov, and D. P. Borisov, Izv. Vyssh. Uchebn. Zaved., Fizika, No. 9, 3 (2011).

Translated by K. Shakhlevich